Supplemental material to this article can be found at:
http://dmd.aspetjournals.org/content/suppl/2015/09/09/dmd.115.064519.DC1

1521-009X/43/12/1882–1890$25.00
Drug Metabolism and Disposition
http://dx.doi.org/10.1124/dmd.115.064519
Drug Metab Dispos 43:1882–1890, December 2015

Insights into the Impact of Heterogeneous Glycosylation on the Pharmacokinetic Behavior of Follistatin-Fc–Based Biotherapeutics

Amita Datta-Mannan, Lihua Huang, Jennifer Pereira, Benjamin Yaden, Andrew Korytko, and Johnny E. Croy

Departments of Drug Disposition Development/Commercialization (A.D.-M.), Biotechnology Discovery Research (J.P., J.E.C), Bioproduct Research and Development (L.H.), and Musculoskeletal Research (B.Y.), Lilly Research Laboratories, Lilly Corporate Center, Indianapolis, Indiana; Biotechnology Discovery Research, Applied Molecular Evolution, San Diego, California (A.K.)

Received March 27, 2015; accepted September 8, 2015

ABSTRACT

Follistatin 315 heparan sulfate-binding deficient mutant human IgG_4 Fc fusion (FST-ΔHBS-Fc) is a follistatin (FST) based Fc fusion protein currently being developed as a novel therapy for several potential indications, including muscle wasting. Previous assessments of the pharmacokinetics and therapeutic activity of FST-ΔHBS-Fc have shown a close association of the exposure–response relationship. The current work builds upon these initial studies by investigating the glycosylation characteristics of FST-ΔHBS-Fc after recombinant expression and its impact on the pharmacokinetics in mice and Cynomolgus monkeys. The data presented indicate that FST-ΔHBS-Fc is heterogeneously glycosylated at the three putative sites in FST when recombinantly expressed in stably transfected Chinese hamster ovary cells. Such carbohydrate heterogeneity, especially with regards to sialic acid incorporation, directly results in sugar-dependent clearance in both mice and Cynomolgus monkeys. Examination of the pharmacokinetics of FST-ΔHBS-Fc molecules containing variable sialic acid content in asialoglycoprotein receptor 1 (ASPGR-1) knockout mice supports the receptor's role as part of the clearance mechanism of the molecules. Based on the evaluation of several variably sialylated lots of material in pharmacokinetic assessments, we define specifications for average sialic acid incorporation into FST-ΔHBS-Fc that result in limited sugar-mediated clearance. Taken together, these studies highlight the importance of establishing an early understanding of the glycosylation/pharmacokinetic relationships of FST-ΔHBS-Fc, which will provide a basis for future application toward optimal systemic drug delivery and dosing strategies.

Introduction

Follistatin (FST) is a regulatory glycoprotein with a myriad of biologic functions in humans (Ueno et al., 1987; Kogure et al., 1995, 1996; Fuwii et al., 2005; Fumagalli et al., 2007; Kota et al., 2009). It is involved in the regulation of early fetal development and cellular differentiation, regulating follicle-stimulating hormone and luteinizing hormone release and action (Carroll et al., 1991; Barakat et al., 2008; Aroua et al., 2012), wound healing (Fumagalli et al., 2007), tissue regeneration and repair, including bone, muscle, and skin (Inoue et al., 1994; Funaba et al., 1996; Gajos-Michniewicz et al., 2010, 2012), and limiting cancer cellular proliferation (Ogino et al., 2008; Tumminello et al., 2010; Karve et al., 2012; Ren et al., 2012; Sepporta et al., 2013). In all cases, these regulatory functions are conferred via its direct engagement with and potent antagonism (and in some cases agonism) of members of the transforming growth factor β (TGFβ)-like family of proteins.

The diverse biologic regulatory properties embodied by FST have spurred considerable interest in developing FST-based therapeutics to treat a wide array of potential indications. Indeed, several groups have reported potent beneficial effects of FST administration in various indications, such as inflammation, liver repair, fibrosis, wound healing, hair regrowth, and muscle disorders, including muscular dystrophy (Kogure et al., 1995; Wankell et al., 2001; Fuwii et al., 2005; Fumagalli et al., 2007; Tsuchida 2008; Zimber et al., 2011; de Kretser et al., 2012; Datta-Mannan et al., 2013).

Although, many studies indicate FST has the potential to be applied to various diseases, the development of FST as a biotherapeutic remains a relatively unexplored frontier. This is likely due to its high degree of molecular complexity, structural properties, and posttranslational glycosylation, which create significant challenges in optimizing the molecule's structure-activity relationship along with its in vivo pharmacokinetic/pharmacodynamic (PK/PD) properties. Human FST, a structurally complex molecule that is composed of 344 residues, is present in two major isoforms that result from alternative mRNA splicing: follistatin 315 (FST315) and follistatin 288 (FST288) (for a review, see Phillips and De Kretser 1998). Both isoforms contain identical core regions that are formed from a series of tandemly repeated domain elements: an N-terminal domain (FST 0), followed by three successive KAZAL/EGF-like repeats units (deemed FST 1, 2, and 3) and a highly acidic C-terminal tail (Keutmann et al., 2004) (Fig. 1). The primary sequence of FST is punctuated by a preponderance of 36 cysteine residues that form 18 disulfide bonds, which interlink the

dx.doi.org/10.1124/dmd.115.064519.
This article has supplemental material available at dmd.aspetjournals.org.

ABBREVIATIONS: ASPGR, asialoglycoprotein receptor; ELISA, enzyme-linked immunosorbent assay; FcRn, neonatal Fc receptor; FST, follistatin; FST288, human follistatin 288 isoform; FST315, human follistatin 315 isoform; FST-Fc, follistatin 315 human IgG_4 Fc fusion; FST-ΔHBS-Fc, follistatin 315 heparan sulfate-binding deficient mutant human IgG_4 Fc fusion; HBS, heparin sulfate-binding sequence; LC/MS, liquid chromatography with mass spectrometry; LLOQ, lower limit of quantitation; MS, mass spectrometry; PBS, phosphate-buffered saline; PD, pharmacodynamic; PK, pharmacokinetic; SCID, severe combined immunodeficient; TGFβ, transforming growth factor β; ULOQ, upper limit of quantitation.

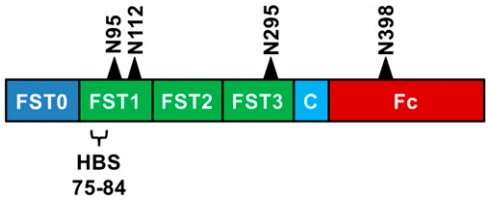

Fig. 1. Domain architecture and location of posttranslationally modified *N*-linked glycosylation sites in FST-ΔHBS-Fc and associated variants. *N*-linked glycosylation sites are designated by solid triangles with corresponding amino acid sites. The native heparin sulfate-binding site (HBS) in FST315 is located in the FST1 domain and comprises a linear stretch of amino acids 75–84 (Sidis et al., 2005).

aforementioned domain elements and stabilize the overall protein structure. Together these various elements provide a structural scaffold that allows FST to interact with TGFβ-like ligands (Thompson et al., 2005; Cash et al., 2009). In addition to providing a ligand-binding surface, the FST 1 domain confers native heparin binding to FST through the presentation of a solvent-accessible heparin sulfate-binding sequence (HBS) (Fig. 1) (Sidis et al., 2005). The complexity of FST is further exacerbated by the presence of three putative *N*-linked glycosylation sites at asparagine residues in positions 95, 112, and 259 (Fig. 1).

In our previous studies, we reported the first published example of the successful engineering of a FST315 variant, deemed follistatin 315 heparan sulfate-binding deficient mutant human IgG_4 Fc fusion (FST-ΔHBS-Fc), which has the potential to serve as a platform for developing a parenterally administered biotherapeutic (Datta-Mannan et al., 2013) in the treatment of diseases where muscle atrophy is implicated (Yaden et al., 2014). In these studies, we fused FST315 to an IgG-derived Fc and removed the protein's intrinsic heparin-binding activity to generate FST-ΔHBS-Fc. After protein engineering, FST-ΔHBS-Fc exhibited ~1600-fold and ~90-fold improvements in exposure and half-life, respectively, in mice relative to unmodified FST315 (Datta-Mannan et al., 2013). This molecule, in contrast to FST315, also displayed robust, dose-dependent pharmacologic effects when administered subcutaneously on a weekly basis in a mouse model of muscle atrophy (Datta-Mannan et al., 2013).

One aspect of FST not covered in our previous studies was the impact of *N*-linked glycosylation on the PK behavior of various FST-ΔHBS-Fc molecules. Heterogeneity in glycosylation is an important consideration when optimizing a glycoprotein for systemic therapeutic use. The main outcome of suboptimal sialylation of solvent exposed *N*-linked glycans in Epo or other glycoproteins (Mortensen and Huseby 1997; Bork et al., 2009; Richards et al., 2010) is recognition and subsequent removal of the compound from circulation via a sugar-based interaction with a specialized subset of lectin-type receptors present on hepatic cells, called the asialoglycoprotein receptors (ASPGRs) (reviewed in Ashwell and Harford 1982).

Given the close association of the exposure–response relationship we observed for FST-ΔHBS-Fc in our previous studies, optimization of the PK properties (and by extension PD) of a FST-based therapeutic must ensure that an optimal glycan character is well characterized and defined. Herein, we present the influence of *N*-linked glycosylation on the PK of two FST-ΔHBS-Fc constructs (deemed MV9 and MV12). First, we found there was a strong correlation between the degree of sialylation with the clearance of the engineered FST-ΔHBS-Fc variants in both mice and Cynomolgus monkeys. Additionally, the examination of the PK of a subset of the FST-ΔHBS-Fc molecules in ASPGR-1 knockout mice further implicated the role of lectin-type receptors in the clearance of these molecules. Significantly, these studies highlight the molecular complexity inherent in the production of recombinant FST from mammalian cell culture and the dependence of in vivo PK properties on the extent and composition of the carbohydrates present on the molecule.

Materials and Methods

Expression and Purification of Recombinant MV9 and MV12 FST-ΔHBS-Fc Proteins. The MV9 and MV12 variants described within this report were expressed in stably transfected Chinese hamster ovary cells and were generated at Eli Lilly (Indianapolis, IN). The primary amino acid sequences for MV9 and MV12 are provided in the supplemental data section of this manuscript (supplemental protein sequences). Isolation of proteins from concentrated cell culture supernatants involved capture by Mab select Sepharose (GE Healthcare, Piscataway, NJ) affinity chromatography, followed (in certain instances) by hydrophobic interaction chromatography, and finally by preparative gel filtration chromatography. These steps generally resulted in protein purity in excess of 98%, as assessed by analytical gel filtration on a TSKgel G3000SWxL column (Tosoh Bioscience, King of Prussia, PA).

Liquid Chromatography with Mass Spectrometry Characterization of Glycosylation Profiles for MV9 and MV12. Liquid chromatography with mass spectrometry (LC/MS) characterization of glycosylation profiles of MV9 and MV12 was conducted for immune affinity captured materials. When murine plasma samples contained at least 400 ng of either MV9 or MV12, the sample was mixed with 15 μl of magnet beads suspension immobilized anti-human IgG4 Fc antibody (4 mg antibody/10 ml of bead suspension) and then incubated at ambient temperature for approximately 100 minutes. Sample beads were then washed with 3 × 100 μl of 1× phosphate-buffered saline (PBS) material was released by incubating with 20 μl and then 10 μl of 20 mM sodium citrate buffer, pH 3.0. Each released solution was mixed with 4 μl of 1 M tris-HCl buffer, pH 8, and 0.5 ml of 50 mg/ml dithiothreitol solution, and then was treated with 1 μl of 0.2 mg/ml Lys-C solution at 37°C for 2 hours. Each digest was alkylated with 1 μl of 100 mg/ml iodoacetamide solution at 37°C for 1 hour and then was mixed with 1 μl of 10% trifluoroacetic acid in H_2O before the LC/MS analysis. Each digest (approximately 5 to 10 μl) was also treated with PNGase F solution to remove N-glycosylation. Mouse plasma spiked with 1 or 20 μg/ml MV9 and MV12 was prepared and treated with the same capture and digest procedures used for the aforementioned mouse samples. For the starting materials, a 20-μl aliquot of 0.5 mg/ml MV9 or MV12 solution was mixed with 80 μl of H_2O and then reduced, digested, and alkylated in a similar way.

Each digest solution was analyzed by a Waters Acquity UPLC (Waters Corporation, Milford, MA) coupled to a ThermoFisher LTQ Orbitrap XL ETD mass spectrometer (ThermoFisher, Waltham, MA). Samples were separated on a Waters Acquity UPLC BEH C18 reversed phase column (1.0 × 100 mm, 1.7 μm particle size) using 0.15% formic acid in water as mobile phase A and 0.12% formic acid in acetonitrile as mobile phase B. The gradient program was as follows: 1% mobile phase B at a flow rate of 100 μl/min at initial and increasing to 8% B in 3.9 minutes, flow rate reduced to 50 μl/min in 0.1 minutes, mobile B increased to 30% in 42 minutes, mobile B increased to 90% at 1 minute, at 90% and increased flow rate to 100 μl with 3 minutes, back to 1% B in 0.5 minutes, and then held at 1% B for 9.5 minutes before the next injection. The eluted sample was introduced into the mass spectrometer through an electrospray ionization source operating at a positive mode with a 15,000 resolution, a scan ion mass range of 250–2000, a spray voltage of 4.0 kV, a capillary temperature of 275°C, a capillary voltage of 3 V, a tube lens of 100 V, and a sheath gas setting of 40 (arbitrary units).

Heparin Sepharose Enzyme-Linked Immunosorbent Assay Binding Assay. The interaction of the MV9 and MV12 FST variants with heparin was measured using a plate-based enzyme-linked immunosorbent assay (ELISA) method. Briefly, heparin-coated binding plates (BD Biosciences, San Jose, CA) were blocked in a solution of casein blocking buffer (Pierce, Rockford, IL) for 1 hour at room temperature. After blocking, the plate was washed once with PBS containing 0.05% Tween 20 and then incubated with varying concentrations of FST-Fc (follistatin 315 human IgG_4 Fc fusion) variants in PBS for 1 hour at room temperature. After incubation, plates were washed with PBS with 0.05% Tween 20 3 times in a plate washer and then incubated with a horseradish peroxidase-conjugated goat-polyclonal anti-human IgG in casein blocking buffer at room temperature for 1 hour. Plates were washed three times, and the signal was developed using one-step ultra TMB-ELISA colorimetric stain, quenched in 2 M

H_2SO_4 and immediately read at 450 nm. Subsequent data were processed using Softmax Pro 4.7 software (Molecular Devices, Sunnyvale, CA).

SMAD-Binding Element 12 (SBE12) Luciferase-Based Reporter Gene Assay. Human embryonic kidney 293 (HEK293) cells stably expressing the SMAD-binding element 12 (SBE12) luciferase system (Qiagen, Venlo, the Netherlands) were seeded 50,000 to 100,000 cells/well/100 μl Dulbecco's modified Eagle's medium/Ham's F12 (Life Technologies, Carlsbad, CA) with 10% fetal bovine serum into a poly-D-lysine coated 96-well plate. After at least 16 hours' incubation at 37°C, the medium was aspirated and replaced with 50 μl of 1% fetal bovine serum–Dulbecco's modified Eagle's medium/Ham's F12. FST variants were serially diluted in (1:2) PBS, pH 7.4, to produce the following titration range: 3000 ng/ml to 23.4 ng/ml. Each concentration was then mixed with an equal volume of 15 ng/ml of activin A (R&D Systems, Minneapolis, MN) or 45 ng/ml growth differentiation factor 8 (GDF8)/myostatin (R&D Systems and/or Eli Lilly, Indianapolis, IN) and was incubated at ambient temperature for 30 minutes, after which 100 μl of the mixture was added to individual wells. Induction of SMAD reporter (i.e., 100% signal) was achieved by either activin A or growth differentiation factor 8/myostatin alone, and negative controls (i.e., 0 background signal) were achieved by vehicle alone.

Plates were incubated at 37°C for 20 hours followed by aspiration and washed once with PBS, pH 7.4. Cells in individual wells were subjected to lysis, and luminescence measured using a GeniosPRO instrument (Tecan, Mannedorf, Switzerland) with substrate injection (Luciferase Reporter Gene Assay Kit; Roche, Basel, Switzerland). Values shown in the figures are representative of transfection experiments performed in triplicate. Relative luciferase units were measured, and IC_{50} curves were fitted using GraphPad Prism software (GraphPad Software, La Jolla, CA).

Murine Pharmacokinetic Studies. Several murine PK studies were conducted at a contract research organization (Covance Laboratories, Madison, WI). The conduct of the animal studies was within the established requirements of the humane animal use standards and guidelines established by Covance. Initially, before conducting the *N*-linked glycosylation profiling, a PK study of FST-ΔHBS-Fc and the two FST-ΔHBS-Fc variants MV9 and MV12 was conducted in male severe combined immunodeficient mice (SCID) (20–30 g) (Harlan, Indianapolis, IN) after a single subcutaneous dose of each molecule dissolved in PBS, pH 7.4, at a dose level of 10 mg/kg.

Subsequently, after *N*-linked glycosylation determination, the PK analyses for FST-ΔHBS-Fc variants characterized with 16%, 27%, 33%, or 60% overall sialic acid starting content were conducted in male SCID mice (20–30 g) (Harlan, Indianapolis, IN), after a single intravenous dose via the tail vein of the variant dissolved in PBS, pH 7.4 at a dose level of 1 mg/kg. Finally, additional PK studies for FST-ΔHBS-Fc molecules containing an overall starting sialic acid content 16% and 60% were also conducted in male and female asialoglycoprotein receptor-1 (ASPGR-1) knockout mice (Jackson Laboratories, Bar Harbor, ME) mice after a single intravenous dose via the tail vein of the FST-ΔHBS-Fc variant dissolved in PBS, pH 7.4, at a dose level of 10 mg/kg.

In the SCID mouse studies, blood samples were collected from three animals per treatment group per time point at 0.083 (intravenous only), 12 (subcutaneous only), 24, 72, 168, 252, 336 420, and 504 hours after administration. Blood samples were collected from two animals per treatment group per time point at 0.083, 6, 48, 96, 168, and 336 hours after administration in the ASPGR-1 knockout mouse study. In each study, the mouse blood samples were collected by saphenous vein, tail clip, retro-orbital, or cardiac puncture into tubes containing sodium EDTA as anticoagulant and processed to plasma.

Cynomolgus Monkey Pharmacokinetic Studies. The Cynomolgus monkey PK study was conducted at a contract research organization (Covance Laboratories). The conduct of the nonhuman primate study was within the established requirements of the humane animal use standards and guidelines established by Covance. Twelve male Cynomolgus monkeys (2 to 5 kg) were assigned to one of four study groups. Each animal received a single intravenous dose of FST-ΔHBS-Fc characterized with 16%, 27%, 33%, or 60% overall starting sialic acid content dissolved in PBS, pH 7.4, at 1 mg/kg. Blood samples were collected from the femoral vein at 0.083, 1, 6, 12, 24, 48, 72, 96, 120, 144, 168, 192, 216, 240, 288, 336, 384, 456, 528, 600, and 672 hours after administration of the dose. Blood samples were allowed to clot at ambient temperature before centrifugation to obtain serum.

Bioanalytic Assays for the Pharmacokinetic Samples and Pharmacokinetic Data Analysis. Concentrations of the FST-ΔHBS-Fc variants with different overall starting sialic acid content in mouse plasma or Cynomolgus monkey serum were determined using mini-validated ELISAs for each of the compounds. Briefly, each well of an Immulon 4 microtiter plate (Thermo Electron, Waltham, MA) was coated with an anti-human FST IgG (R&D Systems) at 4°C overnight. After washing and blocking, standards for each sialic acid variant and its respective samples were added to the wells in a volume of 0.1 ml and incubated for one hour at room temperature. The bound FST-ΔHBS-Fc variants were detected with a horseradish peroxidase-conjugated mouse anti-human IgG (Southern Biotechnology Associates, Birmingham, AL).

The quantitation ranges of the assays for each sialic acid variant were defined as the ability of quality control samples to demonstrate a mean recovery within a 20% coefficient of variation relative to the theoretical concentration in 20% mouse plasma or Cynomolgus monkey serum (in PBS/casein) evaluated at three concentration levels. Based on the precision and accuracy evaluated in these assays, the reportable range was 0.35 to 100 ng/ml in both Cynomolgus monkey serum and mouse plasma for each of the sialic acid variants. The lower limit of quantitation (LLOQ) and upper limit of quantitation (ULOQ) in neat matrix were defined by a mean recovery within 20% of theoretical at a concentration after three freeze/thaw cycles of the stability spiked samples stored at −70°C in neat matrix for each sialic acid construct.

The LLOQ and ULOQ were 0.78 ng/ml and 75 ng/ml in Cynomolgus monkey serum, respectively, for each of the sialic acid variants. The LLOQ and ULOQ in mouse plasma were 1.4 and 75 ng/ml, respectively, for all the constructs. Storage stability at −70°C in neat matrix was established for up to 30 days for each of the variants.

The PK parameters were calculated using the WinNonlin Professional (version 3.2 or 5.2) software package (Pharsight Corporation, Mountain View, CA). The PK parameters from the Cynomolgus monkey serum concentration–time data were calculated using a linear/log trapezoidal noncompartmental analysis model approach based on the statistical moment theory. The PK parameters from the murine plasma concentration–time data were calculated using a linear trapezoidal with linear interpolation noncompartmental analysis model approach, which pools the data and allows the use of all the information from the sparse sampling design leveraged for the murine studies. The parameters calculated included the maximum serum concentration (C_{max}), area under the curve, clearance, and elimination half-life ($t_{1/2}$) when deemed appropriate to report. Statistical significance between mean clearance and half-life values was evaluated by performing a pairwise Tukey-Kramer analysis, and $P < 0.05$ was considered statistically significant.

Results

In Vitro Binding Properties and Pharmacokinetics of the MV9 and MV12 in SCID Mice. In our previously published work, we showed that fusion of FST315 to a Fc fragment of IgG4 and removal of its intrinsic heparin sulfate binding activity resulted in a PK/PD profile that supported parenteral delivery (Datta-Mannan et al., 2013). Though these changes were sufficient to optimize the PK/PD relationship, several of the other molecular characteristics of FST-ΔHBS-Fc, such as poor yields after protein purification, were found to be incompatible with continued for therapeutic development (data not shown). Subsequent engineering efforts yielded two additional FST-ΔHBS-Fc variants, MV9 and MV12, for which these undesired properties had been resolved (data not shown). The heparin-binding properties and in vitro SMAD 2/3 reporter gene assay results for both the MV9 and MV12 variants were found comparable within the limits of the assay to the parental FST-ΔHBS-Fc (Supplemental Fig. 1 and Table 1, respectively).

In addition, we also performed a PK assessment of these two molecules in SCID mice. The average concentration–time profiles for MV9 or MV12 after a single 10 mg/kg subcutaneous administration are shown in Fig. 2. Both molecules displayed a rapid distribution phase followed by a longer elimination phase, characteristic of Fc fusion proteins. When compared with each other, MV12 exhibited an approximate 2-fold higher exposure (area under the curve) relative to MV9 (Table 1).

TABLE 1

Mean pharmacokinetic parameters FST-Fc, MV9, and MV12 in SCID mice after a single 10 mg/kg subcutaneous administration

The plasma concentrations were determined using validated antigen capture ELISAs. Pharmacokinetic parameters were determined from a non-compartmental analysis model. Values in parentheses represent the S.E.M. as calculated by the sparse sampling method used to extract PK parameters.

Protein	C_{max}	T_{max}	AUC_{0-last}
	μg/ml	*H*	*μg·h/ml*
FST-Fc	11.3 (0.7)	24	1092 (38)
MV9	10.7 (1.2)	24	1347 (57)
MV12	36.5 (4.3)	12	2940 (77)

AUC_{0-last}, area under the serum concentration curve from 0 to last concentration versus time point; C_{max}, maximal observed serum concentration; T_{max}, time at which maximal serum concentration was observed.

LC/MS-Based Characterization of Glycosylation Properties in MV9 and MV12. Given the large degree of carbohydrate predicted to be present in MV9 and MV12, we hypothesized that the PK differences observed in between the variants (Fig. 2) may in part be driven by differences in their overall glycosylation attributes. To better understand how glycan heterogeneity influenced the PK properties of MV9 and MV12, we performed an extensive LC/MS-based characterization of the N-linked glycosylation profiles of the starting materials used in the aforementioned murine PK study.

In the first experiment, we examined the sugar occupancies in MV9 and MV12 at each of the predicted sites based on their respective primary amino acid sequences. (Fig. 1). The mass spectrometry LC/MS analyses indicated that each of the predicted FST N-linked sites (N95, N112, N295) as well as the Fc site (N398) in both MV9 and MV12 contained varying carbohydrate occupancies (Supplemental Fig. 2). Although varied in occupancy, each N-linked site in MV9 and MV12 was observed to exhibit a unique preference for a specific carbohydrate antennary structure that was conserved across variants (Supplemental Fig. 3A). Taken together, these results suggest that the gross carbohydrate antennary structural preferences of the FST-ΔHBS-Fc variants are likely governed in a site-specific manner, perhaps by primary amino acid sequence and/or tertiary structures surrounding the *N*-linked attachment sites.

We next used LC/MS to examine the detailed character of the carbohydrate termini present at each *N*-linked site within MV9 and MV12. More specifically, we calculated the ratios of average sialic acid, galactose, and *N*-acetylglucosamine/mannose to oligosaccharide present in the starting materials used in the aforementioned mouse PK study.

Examination of the *N*-linked glycans present in the FST region of both proteins showed that the degree of sialylation was greater in MV12 relative to MV9, resulting in an overall average of 46% more sialic acid per oligosaccharide in MV12 (Fig. 3). It was also noted that in both variants the degree of sialylation at N398 was comparable and low (data not shown). Closer analysis of the asialylated species in both MV9 and MV12 showed that carbohydrate termini preferentially terminated in galactose (Supplemental Fig. 4A), followed by *N*-acetylglucosamine/mannose (Supplemental Fig. 4B).

Given the differences observed in these two proteins, we wanted to understand the impact of lot-to-lot variation on the glycosylation properties of FST-Fc. We therefore characterized by LC/MS the overall average sialylation percentage of 12 independently produced lots of MV9 and MV12 using a fixed cell culture and purification process. Unlike the conservation noted in the average antennary structures (Supplemental Fig. 3A) of these molecules, the degree of site-specific sialylation (Supplemental Fig. 3B) was observed to be highly varied in our expression system. These data suggest that the differential sialylation properties of MV9 and MV12 were most likely the result of lot-to-lot variability in their overall glycosylation properties and not the result of the differences in their overall chemical structures.

Correlation of Pharmacokinetic Properties of MV9 and MV12 with Specific Changes in Glycosylation Attributes. Given the PK differences highlighted in Fig. 2 and Table 1 and the noted differences in the terminal structure of carbohydrate found between MV9 and MV12, we next leveraged our LC/MS assay to determine whether clearance rates of the two proteins could be correlated to starting average sialylation content. For this study, we collected samples of each protein from murine serum at various time points, and we characterized the carbohydrate structures that were present in each variant that exhibited extended circulating half-life. In an effort to address whether any bias was associated with the sample extraction process before the LC/MS analyses, we compared the average molar ratios of each terminal carbohydrate species to 1) the molar amount of oligosaccharide present in the starting unprocessed samples, and 2) that of starting materials spiked into sera and then extracted.

Analysis of these samples indicated that the extraction methodology did not significantly alter the ratios (data not shown). The glycosylation properties as revealed by the LC/MS analysis of subcutaneously injected MV9 and MV12 materials recovered at 0 and 336 hours are

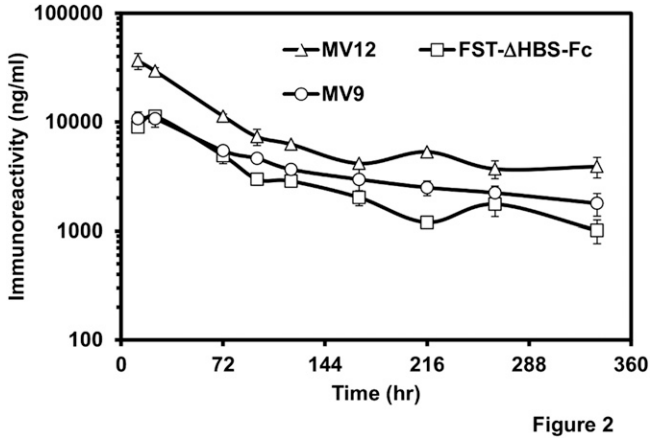

Fig. 2. The pharmacokinetics of FST-Fc and the two FST-ΔHBS-Fc variants MV9 and MV12 in SCID mice after a single 10-mg/kg subcutaneous administration of each protein. Plasma concentrations were determined using a validated ELISA for each molecule. Data represent the mean of three animals/time point for each molecule.

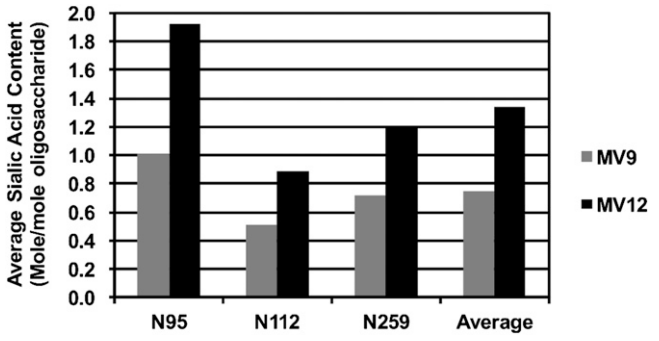

Fig. 3. Comparison of the average molar ratio of carbohydrates terminating in sialic acid in the single lots of MV9 (gray bars) and MV12 (black bars). Data are represented both on a site-to-site comparison and overall global average of the three sites in the FST region of each variant. Inclusion of error bars would be undiscernible due to robustness in triplicate measurement variability and for this reason are not included.

described in Fig. 4. The results show significant changes in the relative ratios of each specific terminus evaluated for both MV9 and MV12. Kinetically, these changes were punctuated by a rapid-compositional change that occurred before the first time point measured in our study (T = 12 hours), after which a slower rate of change was observed (Supplemental Fig. 5, A–F); this was found to be independent of the variant and *N*-linked site evaluated.

Compositionally, we found that each FST *N*-linked site in MV9 (Fig. 4A) and MV12 (Fig. 4B) exhibited an increased proportion of sialylated carbohydrates as circulation time progressed. Conversely, the proportion of terminal galactose and/or *N*-acetylglucosamine/mannose measured decreased as a function of prolonged in vivo exposure for both variants. These changes were not limited to a specific *N*-linked site because similar compositional changes with time were observed independent of attachment site (Fig. 4, A and B).

Overall, a comparative analysis of the degree of change in starting versus terminal circulating sialylated species was ~50% greater in MV9 relative to MV12, which likely reflects the preferential clearance of poorly sialylated species during prolonged circulation. One final observation was that though the carbohydrates present at the Fc-position N398 were found to be largely asialylated (Supplemental Fig. 2), these species were not altered to an appreciable amount during extended circulation in vivo (data not shown). This finding is consistent with other published studies on antibody-therapeutic fusions (Jefferis, 2005).

Pharmacokinetics of MV9 and MV12 Sialic Acid Variants in SCID Mice and Cynomolgus Monkeys. Given the connection between the starting materials sialic acid content and the effect on its PK profile, we further characterized the impact of variable sialic acid content in the FST-ΔHBS-Fc variants by expressing and purifying several independent lots of MV9 and MV12, each containing differential overall average sialic acid content (quantified by LC/MS analysis; Table 2). The PK of the MV9 molecules with varying average sialic acid content were evaluated in both SCID mice and Cynomolgus monkeys; the MV12 proteins were only examined in SCID mice.

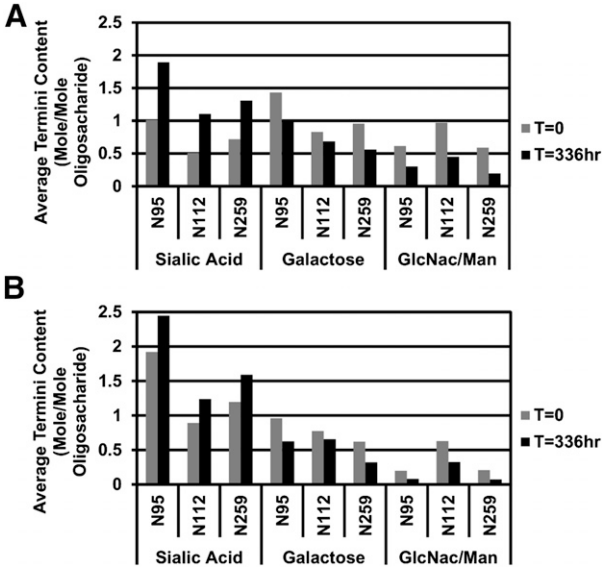

Fig. 4. Comparative summary of the concentrations of specific carbohydrate species terminating in defined structures in FST-ΔHBS-Fc variants MV9 and MV12 after extended in vivo circulation. Individual columns represent the molar ratio of each identified termini [sialic acid, galactose, and *N*-acetylglucosamine] of samples extracted from serum samples taken from the SCID pharmacokinetic study. Data shown are specifically for position N112 and are representative of other sites not shown for (A) MV9 and (B) MV12.

TABLE 2

Pharmacokinetic parameters FST-ΔHBS-Fc sialic acid variants in SCID mice after a single 1-mg/kg intravenous administration

Plasma concentrations were determined using validated antigen capture ELISAs. Pharmacokinetic parameters were determined from a linear trapezoidal with linear interpolation non-compartmental analysis model. Values in parentheses represent the S.E.M. as calculated by the sparse sampling analyses.

FST-ΔHBS-Fc Variant	C_{max}	AUC_{0-last}	CL	V_{ss}	$t_{1/2}$
	μg/ml	*μg·h/ml*	*ml/h/kg*	*ml/kg*	*h*
MV9 16% SA	7.9 (2.1)	400 (23)	2.01	570	277
MV9 27% SA	12.1 (0.3)	546 (15)	1.59	346	200
MV9 33% SA	13.9 (1.2)	681 (19)	1.19	326	247
MV9 60% SA	20.3 (0.7)	1304 (24)	0.64	162	181
MV12 36% SA	12.5 (0.7)	567 (13)	1.49	350	194
MV12 70% SA	17.7 (2.5)	979 (69)	0.75	258	289

AUC_{0-last}, area under the serum concentration curve from 0 to last concentration versus time point; CL, clearance; V_{ss}, volume of distribution at steady state; $t_{1/2}$, elimination half-life.

The results of these studies showed a biphasic clearance profile characterized by a rapid distribution phase followed by a longer elimination phase, consistent with the mouse studies presented above (Fig. 2 and Fig. 5). The average concentration versus time profiles for each MV9 and MV12 variant in SCID mice and/or Cynomolgus monkeys are shown in Figs. 5 and 6, respectively.

When compared with each other, the kinetic profiles of the sialic acid content variants displayed differences in both SCID mice and Cynomolgus monkeys. The MV9 and MV12 sialic acid variants showed mean clearance values ranging from 0.64 to 2.01 ml/h/kg in SCID mice (Table 2) whereas in Cynomolgus monkeys the MV9 sialic acid variants had mean clearance values ranging from 0.95 to 7.47 ml/h/kg (Table 3). Additionally, no antidrug antibodies were detected after administration of any of the variants to Cynomolgus monkey (data not shown). Antidrug antibodies were not measured in the mouse studies given the compromised immune system background of SCID mice.

The sialic acid variants display a pattern of slowed mean clearance with increasing sialic acid content in both species (Figs. 5 and 6; Tables 2 and 3). Pairwise statistical analyses of the monkey data showed statistically significant clearance differences ($P < 0.05$) between the following pairs: 16% and 60% variants, 16% and 33% variants, and 16% and 27% variants. Though statistically significant differences in clearance were not observed for any other pairs, the data suggest a trend for further decreasing clearance with increased average sialic acid content up to 60% (highest tested). Similar trends were observed in the murine data, but due to the nature of the sparse sampling design, no statistical analyses of the murine PK data were performed.

The influence of the overall average sialic acid content differences of the MV9 and MV12 variants' elimination half-life values in SCID mice

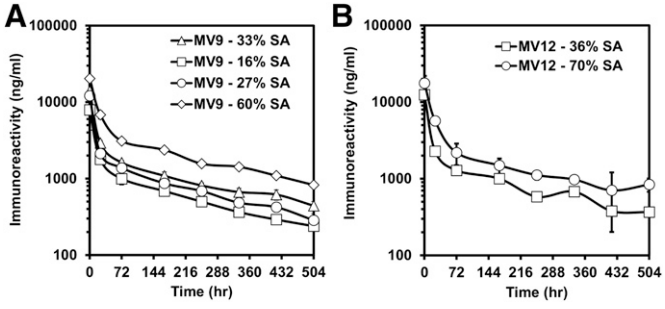

Fig. 5. The pharmacokinetics of the two FST-ΔHBS-Fc initial sialic acid (SA) content variants (A) MV9 and (B) MV12 in SCID mice after a single 1-mg/kg intravenous administration of each protein. Plasma concentrations were determined using a validated ELISA for each molecule. Data are the mean ± S.D. of three animals/time point for each molecule.

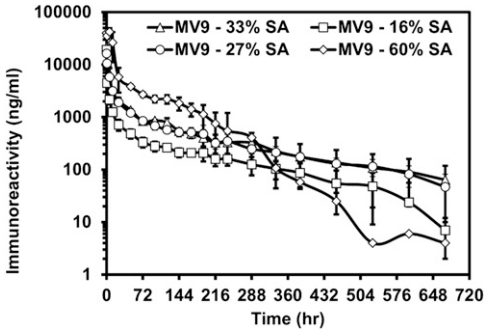

Fig. 6. The pharmacokinetics of MV9 variants with a range of initial sialic acid (SA) content in the Cynomolgus monkey after a single 1-mg/kg intravenous administration of each protein. Plasma concentrations were determined using a validated ELISA for each molecule. Data are the mean ± S.D. of three animals/time point/group for each molecule.

and Cynomolgus monkeys was more marginal that the effects on clearance (Tables 2 and 3). In SCID mice and Cynomolgus monkeys, the half-lives of the variants ranged from ~200 to ~300 hours and ~100 to ~200 hours, respectfully. Pairwise statistical analyses showed no statistically significant differences in half-life between the variants in monkeys. Analysis of the relationship of the average sialic acid content with the in vivo clearance and half-life for the FST-ΔHBS-Fc variants in both SCID mice and/or Cynomolgus monkeys showed there is a reasonably direct correlation with clearance but not elimination half-life (Fig. 7, A–D).

Pharmacokinetics of the MV9 Sialic Acid Variants in ASPGR-1 Knockout Mice. To determine whether the clearance mechanism of the FST-ΔHBS-Fc molecules was due to interaction with a specialized subset of lectin-type receptors present on hepatic cells, we evaluated the PK of a pair of MV9 variants (16% and 60% average sialic acid content) in an ASPGR-1 knockout mouse model. The average concentration–time profile for each MV9 variant in the ASPGR-1 knockout mice is shown in Fig. 8 and Table 4. The MV9 16% and 60% average sialic acid variants showed mean clearance values of 2.3 and 1.4 ml/h/kg, respectively, in ASPGR-1 knockout mice. The elimination half-life for the two variants was not quantified due to the sparse sampling in the terminal phase of the PK profile.

Discussion

Our previous studies investigated the PK/PD responses of various FST-based therapeutics for which a close relationship between these important parameters was revealed (Datta-Mannan et al., 2012). One critical engineering step toward developing a systemically active FST-based therapeutic was achieved by fusing a heparin-binding deficient form of FST344 to the Fc of a murine and/or human IgG (Datta-Mannan et al., 2012). Further investigation of two FST-ΔHBS-Fc variants from this platform is disclosed in this report. Specifically, this report analyzes the change in glycosylation circulation profiles of the MV9 and MV12 variants using LC/MS characterization of materials collected from a head-to-head PK study in SCID mice (Fig. 2).

In these studies, we found that MV12 exhibited an approximate 2-fold slower clearance relative to that of MV9 (Table 1). More striking was the fact that both molecules showed a lower than anticipated exposure (area under the curve) for an Fc fusion protein (Czajkowsky et al., 2012). Possible mechanisms that could account for the clearance profile differences between the therapeutic-Fcs include 1) heparin binding, 2) target-mediated clearance, 3) neonatal Fc receptor (FcRn) interactions, and/or 4) antidrug immune response. Given that both MV9 and MV12 displayed no heparin binding in vitro (Supplemental Fig. 1) and that the predicted targets for FST (i.e., TGFβ-like family members) have low circulating levels in mice (Wu et al., 2012; and unpublished data) it was unlikely that either heparin binding in vivo or binding to target were clearance mechanisms that could explain the PK differences observed. Moreover, formation of antidrug antibodies was also unlikely to account for the observed clearance differences because these PK studies were performed in immune-compromised mice.

Finally, we explored whether the FcRn-binding properties of these variants were involved in their rapid clearance. It is well established that the improved half-life of Fc fusion proteins is, in part, attributable to interactions of the Fc moiety with the neonatal Fc receptor (FcRn), which salvages the proteins from intracellular degradation and promotes recycling of the Fc fusion proteins back into circulation (for a review, see Czajkowsky et al., 2012). Thus, it was also possible that the decrease in FcRn-binding properties of these variants was involved in their rapid clearance; however, comparison of the FcRn-binding interactions of MV9 and MV12 showed no discernable differences (data not shown). In summary, our initial mouse PK data (Fig. 2 and Table 1) suggested that some other biophysical (i.e., stability, charge distribution, aggregation potential, solubility) or biochemical (post-translation modifications, nonspecific binding properties) dissimilarity between the variants were likely influencing their PK. As such, we sought to better understand whether glycosylation could explain the differential PK.

One aspect that has not been characterized in the literature is the impact of glycosylation on the PK properties of FST-based therapeutics, either in a natively glycosylated or recombinant context. Given that native FST344 is predicted (based on primary amino acid sequence) to

TABLE 3

Pharmacokinetic parameters for the FST-ΔHBS-Fc sialic acid variants in Cynomolgus monkeys after a single 1 mg/kg intravenous administration.

Serum concentrations were determined using validated antigen capture ELISAs. Data are the mean ± S.D. of the PK parameters determined from three monkeys per group. Pharmacokinetic parameters were determined from a linear/log trapezoidal non-compartmental analysis model based on the statistical moment theory. Pairwise Tukey-Kramer analysis of mean clearance values indicates that only MV9 16% SA variant was significantly different from other variants tested ($P < 0.05$). Pairwise Tukey-Kramer analysis of mean half-life values indicates no significant difference in any of the variants tested ($P > 0.05$).

FST-ΔHBS-Fc Variant	C_{max}	AUC_{0-last}	CL	V_{ss}	$t_{1/2}$
	μg/ml	*μg·h/ml*	*ml/h/kg*	*ml/kg*	*h*
MV9 16% SA	19.2 ± 1.0	139 ± 34	7.5 ± 2.2	962 ± 113	178 ± 51
MV9 27% SA	16.5 ± 6.7	324 ± 32	3.0 ± 0.4	481 ± 97	188 ± 74
MV9 33% SA	21.4 ± 1.8	347 ± 62	2.9 ± 0.7	402 ± 169	141 ± 64
MV9 60% SA	43.9 ± 5.0	1070 ± 174	1.0 ± 0.2	51 ± 0.1	98 ± 38

AUC_{0-last}, area under the serum concentration curve from 0 to last concentration versus time point; CL, clearance; C_{max}, maximal observed serum concentration; $t_{1/2}$, elimination half-life; V_{ss}, volume of distribution at steady state.

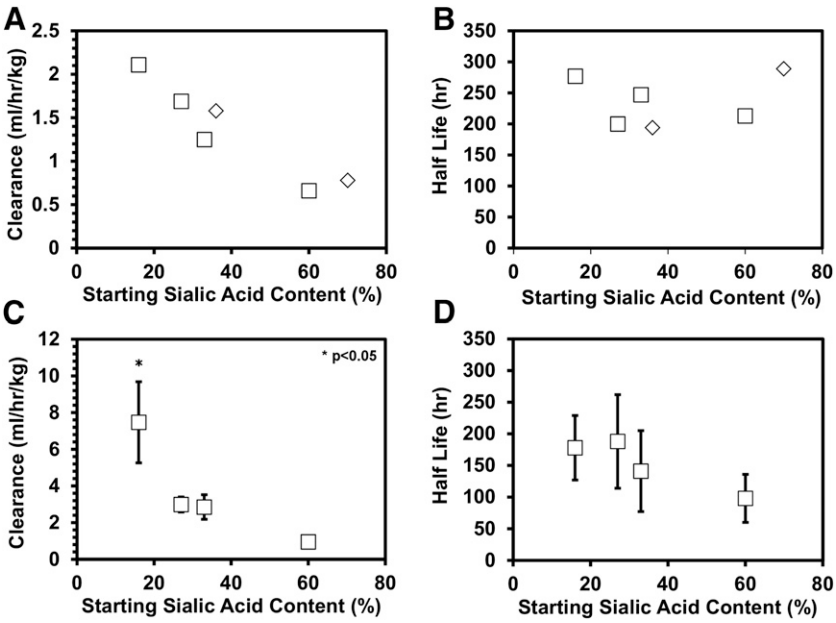

Fig. 7. Relationship between the pharmacokinetic parameters (clearance and half-life) and the MV9 (□) and MV12 (◇) initial sialic acid content variants in (A and B) SCID mice and (C and D) Cynomolgus monkeys after a single 1-mg/kg intravenous administration of each protein in both species. The mean ± S.D. for the pharmacokinetic parameters is shown for monkey. Pairwise Tukey-Kramer analysis of mean clearance values from Cynomolgus monkeys ($n = 3$) indicate that only the MV9 16% SA variant was significantly different from other SA variants tested ($P < 0.05$). Conversely, a pairwise Tukey-Kramer analysis of the same SA variants did not indicate any significant difference in half-life values ($P > 0.05$).

contain up to three *N*-linked glycosylation sites, and in the context of the Fc platform this burden is increased to a total of eight putative sites (six in FST and two in the Fc region), we sought to better understand whether glycosylation heterogeneity could explain the differential PK profiles of MV9 and MV12. Using a LC/MS approach initially reported by Huang et al. (2006), we found that each of the putative sites in the FST regions of MV9 and MV12 were indeed occupied to varying degrees with carbohydrates of heterogeneous structural character. These findings are consistent with a previous report by Hyuga et al. (2004) that evaluated the glycosylation properties of recombinantly expressed and Chinese hamster ovary cell–derived FST288 and FST344. However, one notable difference from these studies observed in our data was the observation that the non-canonical position N112 was found to be variably occupied (Supplemental Fig. 2, specifically peptide 109-118).

The subsequent comparative analysis of MV9 and MV12 samples extracted from serum after prolonged in vivo circulation revealed that molecules containing carbohydrate not terminating in sialic acid were rapidly removed from circulation (Supplemental Fig. 5, A–F). Furthermore, a site-specific comparison of the changes in the distribution of the carbohydrate structure in MV9 and MV12 revealed that no single site contributed more to the clearance of poorly sialylated species; rather, the rapid clearance could be attributed to changes in the average global levels of asialylated carbohydrate as a whole. This is an important distinction as it indicates that engineering to remove individual glycosylation sites would not serve to reduce the observed poor PK properties of FST-ΔHBS-Fc compounds. Rather, the data contends that monitoring of average sialic acid content of carbohydrates is sufficient to inform about the potential influences on the PK profile.

To support this hypothesis, we expressed, purified, and characterized the average sialic acid content of several lots of MV9 and MV12 to determine the impact of sialylation on the PK behavior of FST-ΔHBS-Fc compounds. Indeed, our studies of these differentially sialylated proteins corroborated our hypothesis on the role of terminal glycosylation in affecting the PK of these molecules (Figs. 5 and 6). In mice, both MV9 and MV12 variants containing increased initial sialic acid content were cleared more slowly than the variant molecules containing lower sialic acid content (Fig. 5 and Table 2). We also found that MV9 and MV12 sialic acid variants displayed similar kinetics in vivo when the sialic acid content was similar. These data indicate that the residue differences across MV9 and MV12 within the HBS to reduce heparin-binding impacted the PK similarly.

Thus, in the PK experiments reported herein, the exposure differences between the molecules were predominantly driven by dissimilarities in glycosylation (sialylation) and not by primary amino acid differences. It is worth noting that the examination of the PK of a subset of MV9 sialic acid variants in Cynomolgus monkeys showed findings similar to those in mice, with clearance values increasing for constructs with lower initial sialic acid content (Fig. 6 and Table 3). Additionally, within both species the elimination half-life was similar across the sialic acid variants (Tables 2 and 3). These findings can be explained by the enrichment of optimally sialylated constructs in each population over time. Thus, it is important to understand that although characterization of the average overall sialic acid content of the starting material is a useful and pragmatic approach to estimate clearance properties, each lot of protein is still heterogeneous and contains molecules with variable sialylation.

The negative impact of suboptimal sialylation on the PK behavior of FST-ΔHBS-Fc molecules is a theme that has been explored in other

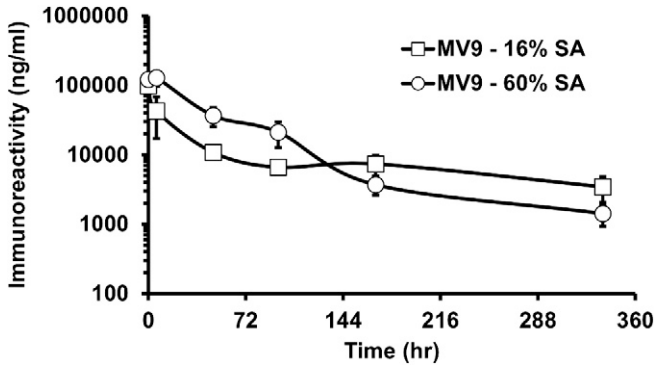

Fig. 8. The pharmacokinetics of two MV9 variants with either 16% or 60% average sialic acid (SA) content in ASPGR-1 knockout mice after a single 10 mg/kg intravenous administration of each protein. Plasma concentrations were determined using a validated ELISA for each molecule. Data are the mean of two animals/time point for each molecule.

TABLE 4

Pharmacokinetic parameters FST-ΔHBS-Fc sialic acid variants in ASPGR-1 knockout mice after a single 10 mg/kg intravenous administration

Plasma concentrations were determined using validated antigen capture ELISAs. Pharmacokinetic parameters were determined from a linear trapezoidal with linear interpolation noncompartmental analysis model. Values in parentheses represent the S.E.M. as calculated by the sparse sampling analyses.

FST-ΔHBS-Fc Variant	C_{max}	AUC_{0-last}	$AUC_{0-\infty}$	CL
	μg/ml	*μg·h/ml*	*μg·h/ml*	*ml/h/kg*
MV9 16% SA	98 (23)	3369 (298)	4343	2.3
MV9 60% SA	136 (16)	7131 (577)	7248	1.4

AUC_{0-last}, area under the serum concentration curve from 0 to last concentration versus time point; $AUC_{0-\infty}$, area under the serum concentration curve from time zero extrapolated to infinite time; CL, clearance; C_{max}, maximal observed serum concentration.

glycotherapeutics and is an important consideration for future development of systemically acting FST-based therapies. Specifically, several studies exploring the clearance attributes (Webster et al., 2003, 2006) of UK-279,276, a glycosylated recombinant neutrophil inhibitor factor, has strongly implicated a potential clearance mechanism that involves the binding and subsequent removal of poorly sialylated species via an avidity-driven interaction with specialized hepatic lectins called the asialoglycoprotein receptors (ASPGR) (Weiss and Ashwell 1989; Spiess 1990; Stockert 1995).

Based on the similarities in our findings with those reported for UK-279,276, we performed a limited PK assessment of two MV9 sialic variants containing either a low (~16%) or high (~60%) average sialic acid content in ASPGR-1 knockout mice to provide a mechanistic explanation of our findings (Fig. 8 and Table 4). Indeed, in SCID mice and Cynomolgus monkeys the ~60% sialic acid variant exhibited an ~3.1-fold and ~7.5-fold slower clearance relative to the ~16% sialic acid variant, respectively. This difference in clearance was reduced to ~1.6-fold in the ASPGR-1 knockout mice. The reduced clearance difference between the variants in the knockout mice relative to SCID mice supports the notion of ASPGR-1 as a route of clearance for FST-ΔHBS-Fc. However, it is important to note that we used a higher dose in our PK evaluations of the variants in knockout mice (10 mg/kg) relative to the SCID mice (1 mg/kg), which may have influenced our exposure findings.

Therefore, a deeper understanding of exposure linearity across dose levels within mice is needed to more fully interrogate the role of ASPGR-1 in the clearance of our molecules. It is also possible that other underdetermined attributes (i.e., charge distribution, aggregation potential, hydrophobicity, and solubility differences) may influence the PK behavior of these molecules, as has been reported recently for other biologics. Interestingly, we also noted that, for reasons unknown to us, the effect of the variable sialylation on the clearance was more pronounced in monkeys than in mice for the MV9 constructs (compare Fig. 5 with Fig. 6, and compare Table 2 with Table 3). These findings were not related to antidrug antibodies affecting the clearance of the molecules in Cynomolgus monkeys (data not shown). These observations may indicate that the ASPGR-1 mechanism plays a greater role in the higher species relative to the rodent. It is also possible that the physiochemical properties of the molecules lead to some differences in nonspecific or unintended binding across the species, which was not assessed within the context of our current efforts. Further studies are required to determine these underlying aspects of the species differences in FST-ΔHBS-Fc PK behavior.

In summary, our previous work (Datta-Mannan et al., 2013) and current studies highlight the exquisite importance of understanding the interplay between heparin binding and glycosylation on the overall PK properties of FST-based therapies. The current studies in this report indicate that the residue differences between MV9 and MV12 within the HBS to reduce heparin binding impacted the PK similarly, and the observed PK differences between the two molecular platforms were predominantly driven by differences in glycosylation (sialylation) and not primary amino acid differences. Furthermore, these studies serve to illustrate the extreme degree of molecular complexity inherent in the production of recombinant FST from mammalian cell culture, and its intimate association with in vivo PK and by extension PD.

Our findings strongly support the importance of careful and thorough glycosylation characterization of these recombinant proteins for a richer understanding of in vivo pharmacology data. Studies to fully determine the implications of the glycosylation profile on the PK/PD relationship are warranted to help guide the selection of the optimal sialylation profile. In addition, future studies should also be considered for a thorough characterization of additional biophysical properties such as the distribution of charge and hydrophobic patches with solvent exposed regions for determining attributes in FST-based glycotherapeutics that inform optimal systemic drug delivery and dosing strategies for the intended pharmacologic application.

Acknowledgments

The authors thank Amber Peariso, Victor Wroblewski, and John Beals for thoughtful discussions on experimental design; Pat Eacho and Krista Schroeder for aid in performing the ASPGR-1 knockout mouse studies; Joe Berry, Joe Swartling, and Jerry Kelly for expression and purification support; Robin Brown, Selina Estwick, Emmanuel Lozano, and Andrea Sperry for conducting pharmacokinetic sample analyses; Stacey Lee for conducting heparin binding assays; Xuhao Yang and Yan Wang for performing SMAD binding assays; Tammy Tuley for LC/MS analysis support on glycan characterization of various follistatin preparations; and Carrie Croy for evaluation of editorial advice on the manuscript.

Authorship Contributions

Participated in research design: Datta-Mannan, Huang, Yaden, Korytko, Croy.

Conducted experiments: Datta-Mannan, Huang, Pereira, Yaden, Korytko, Croy.

Contributed new reagents or analytic tools: Pereira, Korytko, Croy.

Performed data analysis: Datta-Mannan, Huang, Croy.

Wrote or contributed to the writing of the manuscript: Datta-Mannan, Huang, Pereira, Yaden, Korytko, Croy.

References

Aroua S, Maugars G, Jeng SR, Chang CF, Weltzien FA, Rousseau K, and Dufour S (2012) Pituitary gonadotropins FSH and LH are oppositely regulated by the activin/follistatin system in a basal teleost, the eel. *Gen Comp Endocrinol* **175**:82–91.

Ashwell G and Harford J (1982) Carbohydrate-specific receptors of the liver. *Annu Rev Biochem* **51**:531–554.

Barakat B, O'Connor AE, Gold E, de Kretser DM, and Loveland KL (2008) Inhibin, activin, follistatin and FSH serum levels and testicular production are highly modulated during the first spermatogenic wave in mice. *Reproduction* **136**:345–359.

Bork K, Horstkorte R, and Weidemann W (2009) Increasing the sialylation of therapeutic glycoproteins: the potential of the sialic acid biosynthetic pathway. *J Pharm Sci* **98**:3499–3508.

Carroll RS, Kowash PM, Lofgren JA, Schwall RH, and Chin WW (1991) In vivo regulation of FSH synthesis by inhibin and activin. *Endocrinology* **129**:3299–3304.

Cash JN, Rejon CA, McPherron AC, Bernard DJ, and Thompson TB (2009) The structure of myostatin:follistatin 288: insights into receptor utilization and heparin binding. *EMBO J* **28**: 2662–2676.

Czajkowsky DM, Hu J, Shao Z, and Pleass RJ (2012) Fc-fusion proteins: new developments and future perspectives. *EMBO Mol Med* **4**:1015–1028.

Datta-Mannan A, Yaden B, Krishnan V, Jones BE, and Croy JE (2013) An engineered human follistatin variant: insights into the pharmacokinetic and pharmacodynamic relationships of a novel molecule with broad therapeutic potential. *J Pharmacol Exp Ther* **344**:616–623.

de Kretser DM, O'Hehir RE, Hardy CL, and Hedger MP (2012) The roles of activin A and its binding protein, follistatin, in inflammation and tissue repair. *Mol Cell Endocrinol* **359**: 101–106.

Fumagalli M, Musso T, Vermi W, Scutera S, Daniele R, Alotto D, Cambieri I, Ostorero A, Gentili F, and Caposio P, et al. (2007) Imbalance between activin A and follistatin drives postburn hypertrophic scar formation in human skin. *Exp Dermatol* **16**:600–610.

Funaba M, Ogawa K, Murata T, Fujimura H, Murata E, Abe M, Takahashi M, and Torii K (1996) Follistatin and activin in bone: expression and localization during endochondral bone development. *Endocrinology* **137**:4250–4259.

Fuwii M, Ishikawa M, Iuchi M, and Tashiro S (2005) Effect of follistatin on rat liver regeneration and tumor growth after portal occlusion. *Hepatogastroenterology* **52**:833–838.
Gajos-Michniewicz A, Pawlowska E, Ochedalski T, and Piastowska-Ciesielska A (2012) The influence of follistatin on mechanical properties of bone tissue in growing mice with overexpression of follistatin. *J Bone Miner Metab* **30**:426–433.
Gajos-Michniewicz A, Piastowska AW, Russell JA, and Ochedalski T (2010) Follistatin as a potent regulator of bone metabolism. *Biomarkers* **15**:563–574.
Huang L, Biolsi S, Bales KR, and Kuchibhotla U (2006) Impact of variable domain glycosylation on antibody clearance: an LC/MS characterization. *Anal Biochem* **349**:197–207.
Hyuga M, Itoh S, Kawasaki N, Ohta M, Ishii A, Hyuga S, and Hayakawa T (2004) Analysis of site-specific glycosylation in recombinant human follistatin expressed in Chinese hamster ovary cells. *Biologicals* **32**:70–77.
Inoue S, Orimo A, Hosoi T, Ikegami A, Kozaki K, Ouchi Y, Nomura S, Muramatsu M, and Orimo H (1994) Demonstration of activin-A in arteriosclerotic lesions. *Biochem Biophys Res Commun* **205**:441–448.
Jefferis R (2005) Glycosylation of recombinant antibody therapeutics. *Biotechnol Prog* **21**: 11–16.
Karve TM, Preet A, Sneed R, Salamanca C, Li X, Xu J, Kumar D, Rosen EM, and Saha T (2012) BRCA1 regulates follistatin function in ovarian cancer and human ovarian surface epithelial cells. *PLoS One* **7**:e37697.
Keutmann HT, Schneyer AL, and Sidis Y (2004) The role of follistatin domains in follistatin biological action. *Mol Endocrinol* **18**:228–240.
Kogure K, Omata W, Kanzaki M, Zhang YQ, Yasuda H, Mine T, and Kojima I (1995) A single intraportal administration of follistatin accelerates liver regeneration in partially hepatectomized rats. *Gastroenterology* **108**:1136–1142.
Kogure K, Zhang YQ, Kanzaki M, Omata W, Mine T, and Kojima I (1996) Intravenous administration of follistatin: delivery to the liver and effect on liver regeneration after partial hepatectomy. *Hepatology* **24**:361–366.
Kota J, Handy CR, Haidet AM, Montgomery CL, Eagle A, Rodino-Klapac LR, Tucker D, Shilling CJ, Therlfall WR, and Walker CM, et al. (2009) Follistatin gene delivery enhances muscle growth and strength in nonhuman primates. *Sci Transl Med* **1**:6ra15.
Mortensen B and Huseby NE (1997) Clearance of circulating gamma-glutamyltransferase by the asialoglycoprotein receptor. Enzyme forms with different sialic acid content are eliminated at different clearance rates and without apparent desialylation. *Clin Chim Acta* **258**:47–58.
Ogino H, Yano S, Kakiuchi S, Muguruma H, Ikuta K, Hanibuchi M, Uehara H, Tsuchida K, Sugino H, and Sone S (2008) Follistatin suppresses the production of experimental multiple-organ metastasis by small cell lung cancer cells in natural killer cell-depleted SCID mice. *Clin Cancer Res* **14**:660–667.
Phillips DJ and de Kretser DM (1998) Follistatin: a multifunctional regulatory protein. *Front Neuroendocrinol* **19**:287–322.
Ren P, Chen FF, Liu HY, Cui XL, Sun Y, Guan JL, Liu ZH, Liu JG, and Wang YN (2012) High serum levels of follistatin in patients with ovarian cancer. *J Int Med Res* **40**:877–886.
Richards AA, Colgrave ML, Zhang J, Webster J, Simpson F, Preston E, Wilks D, Hoehn KL, Stephenson M, and Macdonald GA, et al. (2010) Sialic acid modification of adiponectin is not required for multimerization or secretion but determines half-life in circulation. *Mol Endocrinol* **24**:229–239.
Sepporta MV, Tumminello FM, Flandina C, Crescimanno M, Giammanco M, La Guardia M, di Majo D, and Leto G (2013) Follistatin as potential therapeutic target in prostate cancer. *Target Oncol* **8**:215–223.
Sidis Y, Schneyer AL, and Keutmann HT (2005) Heparin and activin-binding determinants in follistatin and FSTL3. *Endocrinology* **146**:130–136.
Spiess M (1990) The asialoglycoprotein receptor: a model for endocytic transport receptors. *Biochemistry* **29**:10009–10018.
Stockert RJ (1995) The asialoglycoprotein receptor: relationships between structure, function, and expression. *Physiol Rev* **75**:591–609.
Thompson TB, Lerch TF, Cook RW, Woodruff TK, and Jardetzky TS (2005) The structure of the follistatin:activin complex reveals antagonism of both type I and type II receptor binding. *Dev Cell* **9**:535–543.
Tsuchida K (2008) Myostatin inhibition by a follistatin-derived peptide ameliorates the pathophysiology of muscular dystrophy model mice. *Acta Myol* **27**:14–18.
Tumminello FM, Badalamenti G, Fulfaro F, Incorvaia L, Crescimanno M, Flandina C, Sepporta MV, and Leto G (2010) Serum follistatin in patients with prostate cancer metastatic to the bone. *Clin Exp Metastasis* **27**:549–555.
Ueno N, Ling N, Ying SY, Esch F, Shimasaki S, and Guillemin R (1987) Isolation and partial characterization of follistatin: a single-chain Mr 35,000 monomeric protein that inhibits the release of follicle-stimulating hormone. *Proc Natl Acad Sci USA* **84**:8282–8286.
Wankell M, Munz B, Hübner G, Hans W, Wolf E, Goppelt A, and Werner S (2001) Impaired wound healing in transgenic mice overexpressing the activin antagonist follistatin in the epidermis. *EMBO J* **20**:5361–5372.
Webster R, Edgington A, Phipps J, and Walker D (2006) Pharmacokinetics and clearance processes of UK-279,276 (rNIF) in rat and dog: comparison with human data. *Xenobiotica* **36**:341–349.
Webster R, Phipps J, Hyland R, and Walker D (2003) Evaluation of the role of the asialoglycoprotein receptor in the clearance of UK-279,276 (recombinant neutrophil inhibitory factor). *Xenobiotica* **33**:945–956.
Weiss P and Ashwell G (1989) The asialoglycoprotein receptor: properties and modulation by ligand. *Prog Clin Biol Res* **300**:169–184.
Wu H, Chen Y, Winnall WR, Phillips DJ, and Hedger MP (2012) Acute regulation of activin A and its binding protein, follistatin, in serum and tissues following lipopolysaccharide treatment of adult male mice. *Am J Physiol Regul Integr Comp Physiol* **303**:R665–R675.
Yaden BC, Croy JE, Wang Y, Wilson JM, Datta-Mannan A, Shetler P, Milner A, Bryant HU, Andrews J, and Dai G, et al. (2014) Follistatin: a novel therapeutic for the improvement of muscle regeneration. *J Pharmacol Exp Ther* **349**:355–371.
Zimber MP, Ziering C, Zeigler F, Hubka M, Mansbridge JN, Baumgartner M, Hubka K, Kellar R, Perez-Meza D, and Sadick N, et al. (2011) Hair regrowth following a Wnt- and follistatin containing treatment: safety and efficacy in a first-in-man phase 1 clinical trial. *J Drugs Dermatol* **10**:1308–1312.

Address correspondence to: Johnny E. Croy, Lilly Research Laboratories, Eli Lilly & Company, Lilly Corporate Center, Indianapolis, IN 46285. E-mail: croy_johnny_eugene@lilly.com

SUPPLEMENTAL PROTEIN SEQUENCES

FST-ΔHBS-FC-MV9

GNCWLRQAKNGRCQVLYKTELSKEECCSTGRLSTSWTEEDVNDNTLFKWMIFNGGA

PNCIPCKETCENVDCGPGQSCVVDQTGHPRCVCAPDCSNITWKGPVCGLDGKTYRN

ECALLKARCKEQPELEVQYQGRCKKTCRDVFCPGSSTCVVDQTNNAYCVTCNRICPE

PASSEQYLCGNDGVTYSSACHLRKATCLLGRSIGLAYEGKCIKAKSCEDIQCTGGKKC

LWDFKVGRGRCSLCDELCPDSKSDEPVCASDNATYASECAMKEAACSSGVLLEVKHS

GSCNSISEDTEEEEEDEDQDYSFPGGGGSGGGGSAESKYGPPCPPCPAPEAAGGPS

VFLFPPKPKDTLMISRTPEVTCVVVDVSQEDPEVQFNWYVDGVEVHNAKTKPREEQF

NSTYRVVSVLTVLHQDWLNGKEYKCKVSNKGLPSSIEKTISKAKGQPREPQVYTLPPS

QEEMTKNQVSLTCLVKGFYPSDIAVEWESNGQPENNYKTTPPVLDSDGSFFLYSRLTV

DKSRWQEGNVFSCSVMHEALHNHYTQKSLSLSLG

FST-ΔHBS-FC-MV12

GNCWLRQAKNGRCQVLYKTELSKEECCSTGRLSTSWTEEDVNDNTLFKWMIFNGGA

PNCIPCKETCENVDCGPGRSCVVDQHGRPRCVCAPDCSNITWKGPVCGLDGKTYRN

ECALLKARCKEQPELEVQYQGRCKKTCRDVFCPGSSTCVVDQTNNAYCVTCNRICPE

PASSEQYLCGNDGVTYSSACHLRKATCLLGRSIGLAYEGKCIKAKSCEDIQCTGGKKC

LWDFKVGRGRCSLCDELCPDSKSDEPVCASDNATYASECAMKEAACSSGVLLEVKHS

GSCNSISEDTEEEEEDEDQDYSFPGGGGSGGGGSAESKYGPPCPPCPAPEAAGGPS

VFLFPPKPKDTLMISRTPEVTCVVVDVSQEDPEVQFNWYVDGVEVHNAKTKPREEQF

NSTYRVVSVLTVLHQDWLNGKEYKCKVSNKGLPSSIEKTISKAKGQPREPQVYTLPPS

QEEMTKNQVSLTCLVKGFYPSDIAVEWESNGQPENNYKTTPPVLDSDGSFFLYSRLTV

DKSRWQEGNVFSCSVMHEALHNHYTQKSLSLSLG

SUPPLEMENTAL FIGURE LEGENDS

Supplemental Figure 1: ELISA analysis of FST-Fc (open circles), FST-ΔHBS-Fc (open squares), MV9 (open triangles) and MV12 (open diamonds) interactions with surface coated Heparin Sulfate.

Supplemental Figure 2: Comparison of the relative abundance of the glycosylation occupancy, antennary and structural differences in each of the N-linked sites in MV9 (grey bars) and MV12 (black bars). Data is presented as a relative abundance of oligosaccharide species relative to the total oligosaccharide measured at a given site. Error bars represent the standard deviation in sample measurement obtained by triplicate LCMS measurements.

Supplemental Figure 3: Analysis of the variability in the average antennary structure (A) and percent of asiaylated carbohydrate (B) of the three site-specific N-linked carbohydrates found in the FST-Fc proteins. Average values were calculated from the independent bioreactor productions of MV9 (N=9) and MV12 (N=4) and associated error bars represent the standard deviation in these values taken from LCMS analysis of carbohydrate antennary structure at each given site.

Supplemental Figure 4: Relative comparison of average amounts of carbohydrate content terminating in (A) galactose and (B) n-acetylglucosamine/mannose. Data is

plotted as a function of molar ratio of observed termini relative to molar amount of oligosaccharide observed at each given site in the FST region of MV9 (grey bars) and MV12 (black bars). Average values are provided to understand the differences on a global scale.

Supplemental Figure 5: Changes in molar carbohydrate content of carbohydrates terminating in sialic acid (open circles), galactose (open diamonds) and n-acetylglucosamine (open squares) of samples extracted from serum samples taken from the SCID pharmacokinetic study. Data shown is specifically for position N95 for (A) MV9 and (B) MV12, position N112 for (C) MV9 and (D) MV12 and position N259 for (E) MV9 and (F) MV12.

Title: Insights into the Impact of Heterogeneous Glycosylation on the Pharmacokinetic Behavior of Follistatin-Fc Based Biotherapeutics
Authors: Amita Datta-Mannan, Lihua Huang, Jennifer Pereira, Benjamin Yaden, Andrew Korytko, and Johnny E. Croy
Journal: Drug Metabolism And Disposition
Supplemental Figure 1

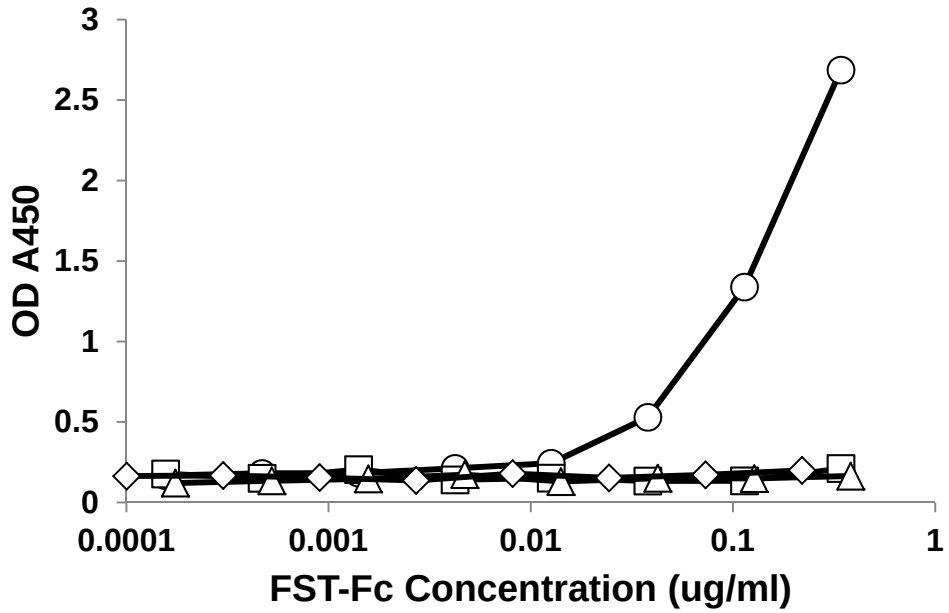

Title: Insights into the Impact of Heterogeneous Glycosylation on the Pharmacokinetic Behavior of Follistatin-Fc Based Biotherapeutics
Authors: Amita Datta-Mannan, Lihua Huang, Jennifer Pereira, Benjamin Yaden, Andrew Korytko, and Johnny E. Croy
Journal: Drug Metabolism And Disposition
Supplemental Figure 2

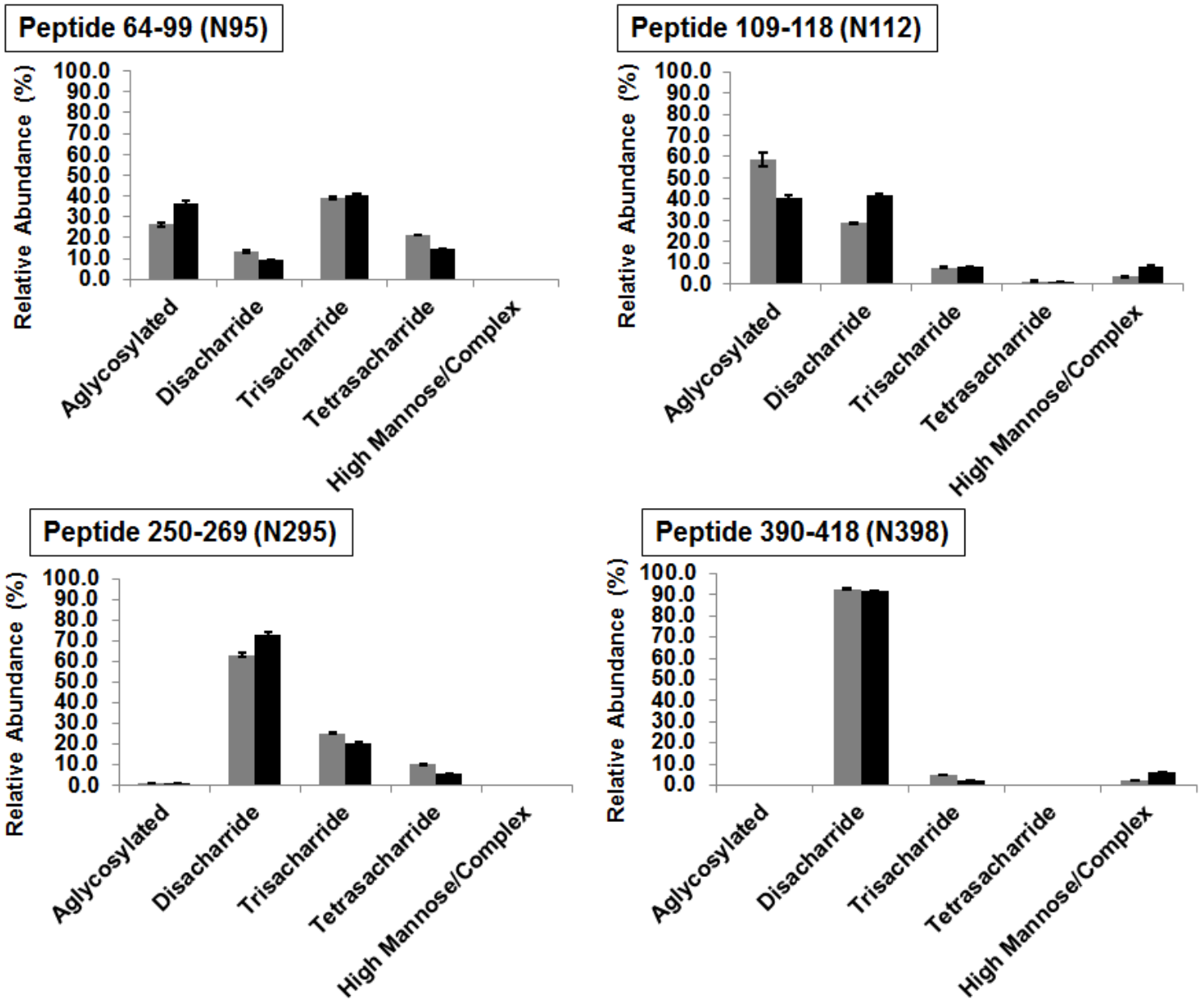

Title: Insights into the Impact of Heterogeneous Glycosylation on the Pharmacokinetic Behavior of Follistatin-Fc Based Biotherapeutics
Authors: Amita Datta-Mannan, Lihua Huang, Jennifer Pereira, Benjamin Yaden, Andrew Korytko, and Johnny E. Croy
Journal: Drug Metabolism And Disposition
Supplemental Figure 3A and 3B

A.

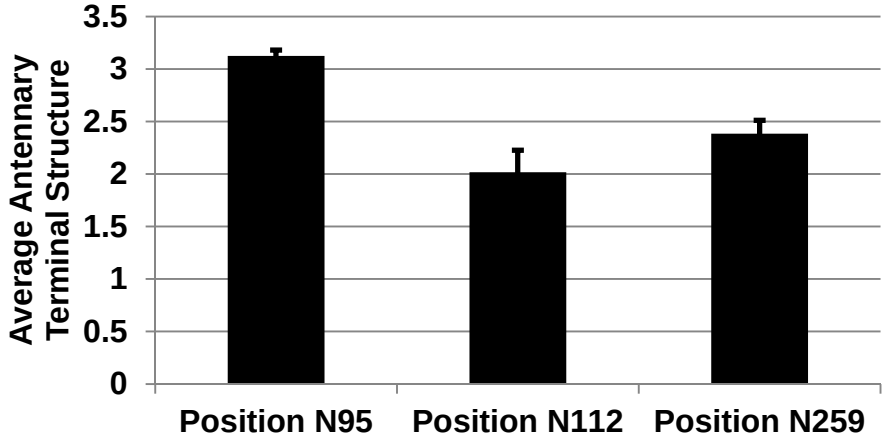

B.

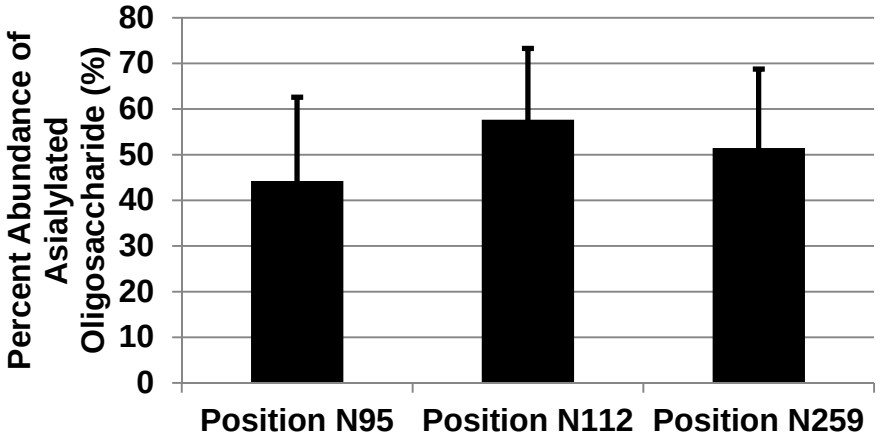

Title: Insights into the Impact of Heterogeneous Glycosylation on the Pharmacokinetic Behavior of Follistatin-Fc Based Biotherapeutics
Authors: Amita Datta-Mannan, Lihua Huang, Jennifer Pereira, Benjamin Yaden, Andrew Korytko, and Johnny E. Croy
Journal: Drug Metabolism And Disposition
Supplemental Figure 4A and 4B

A.

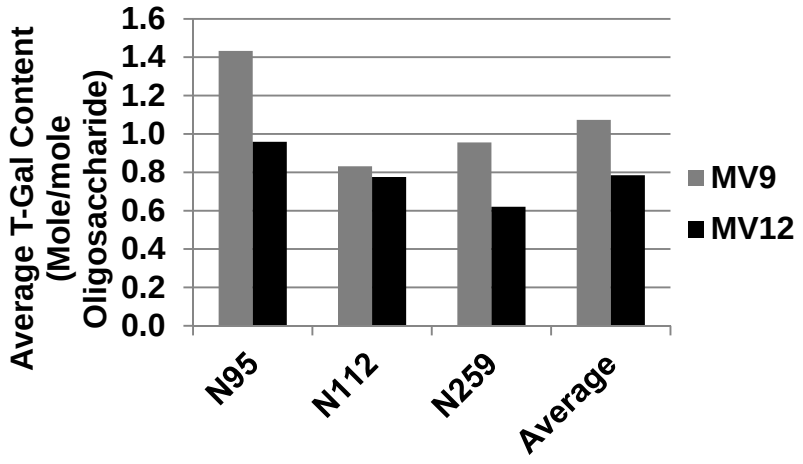

B.

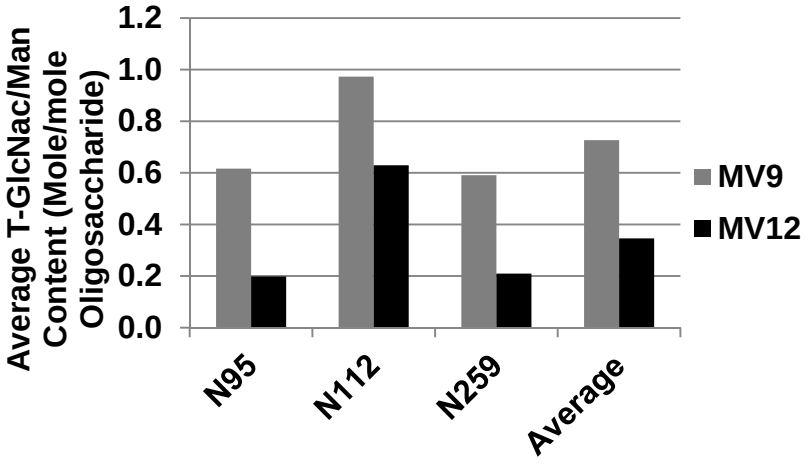

Title: Insights into the Impact of Heterogeneous Glycosylation on the Pharmacokinetic Behavior of Follistatin-Fc Based Biotherapeutics
Authors: Amita Datta-Mannan, Lihua Huang, Jennifer Pereira, Benjamin Yaden, Andrew Korytko, and Johnny E. Croy
Journal: Drug Metabolism And Disposition
Supplemental Figure 5A and 5B

A.

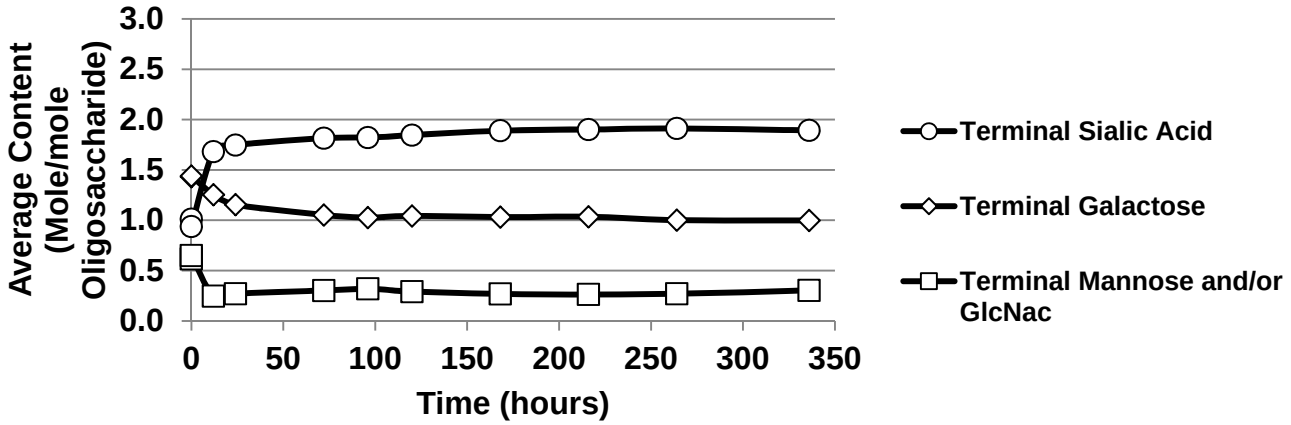

B.

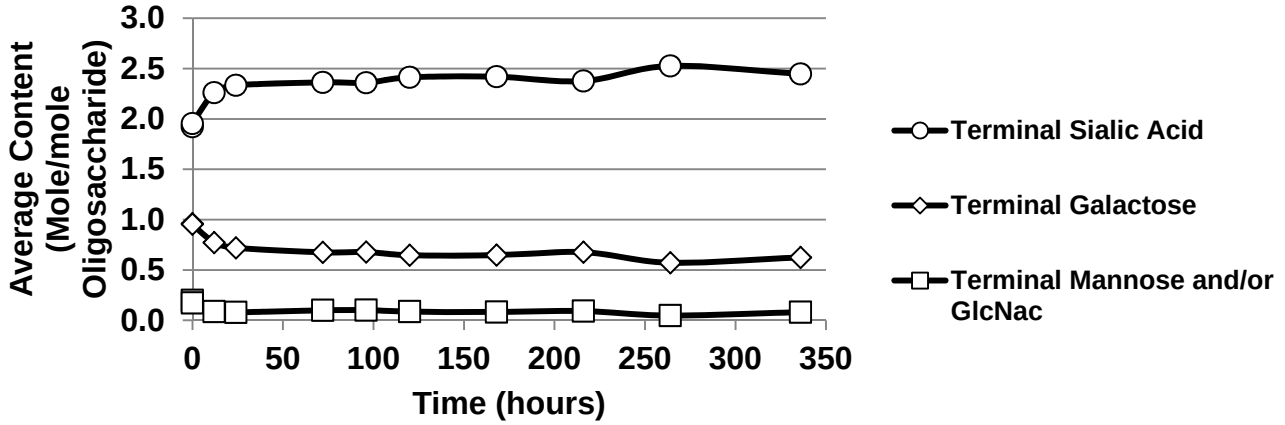

Title: Insights into the Impact of Heterogeneous Glycosylation on the Pharmacokinetic Behavior of Follistatin-Fc Based Biotherapeutics
Authors: Amita Datta-Mannan, Lihua Huang, Jennifer Pereira, Benjamin Yaden, Andrew Korytko, and Johnny E. Croy
Journal: Drug Metabolism And Disposition
Supplemental Figure 5C and 5D

C.

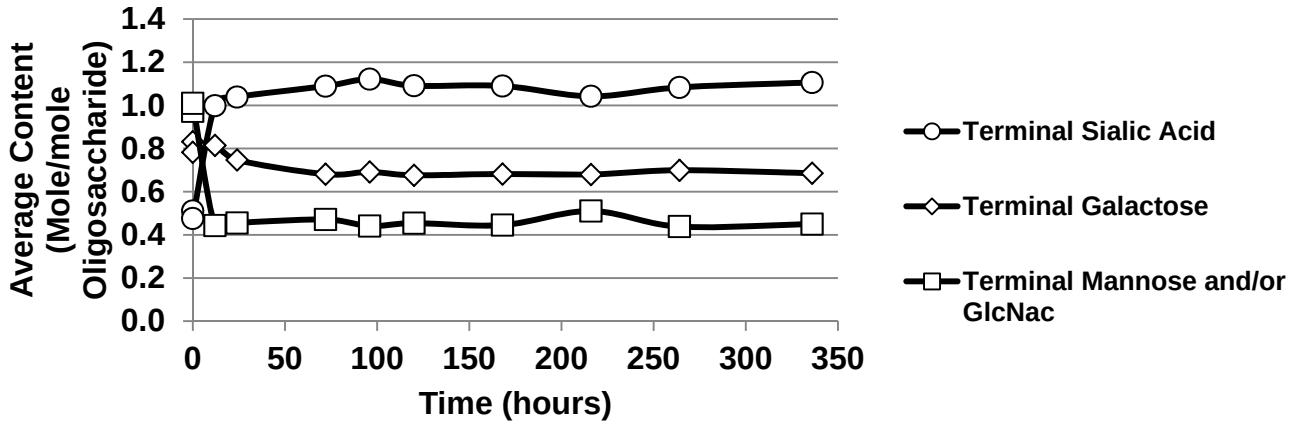

D.

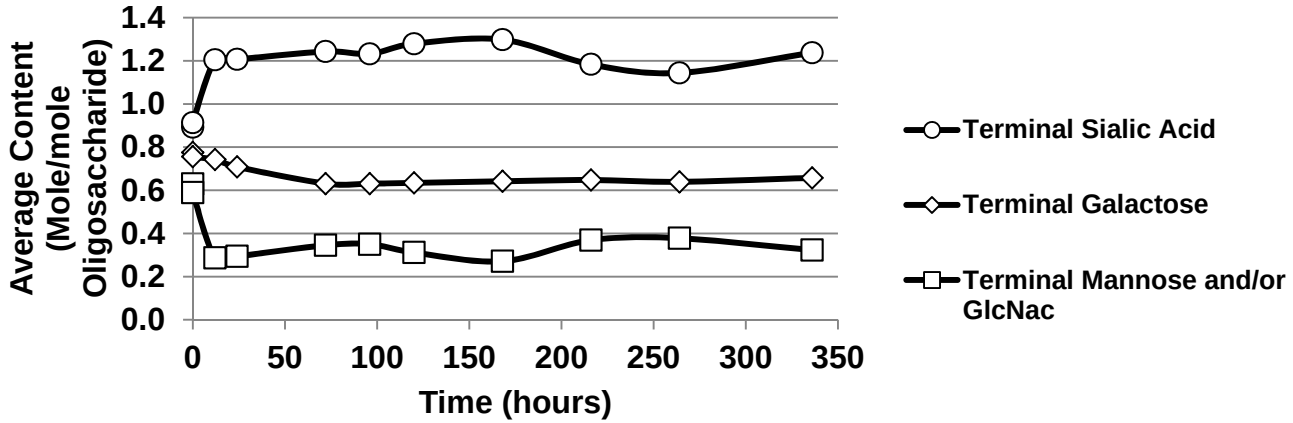

Title: Insights into the Impact of Heterogeneous Glycosylation on the Pharmacokinetic Behavior of Follistatin-Fc Based Biotherapeutics
Authors: Amita Datta-Mannan, Lihua Huang, Jennifer Pereira, Benjamin Yaden, Andrew Korytko, and Johnny E. Croy
Journal: Drug Metabolism And Disposition
Supplemental Figure 5E and 5F